Drive-by damage detection in bridges using the apparent profile

E.J. OBrien[a,1] and J. Keenahan[a,2]
[a] School of Civil, Structural and Environmental Engineering
University College Dublin
Newstead
Belfield
Dublin 4
Ireland

Phone: [1] +363-1-7163224 / [2] +353-1-7163233
Fax: [1,2] +353-1-7163297
Email: [1] eugene.obrien@ucd.ie, [2] jennifer.ni-choinneachain@ucdconnect.ie

Abstract

The concept of using sensors on a passing vehicle, rather than on the bridge, is known as 'Drive-by' damage detection. The newly developed Traffic Speed Deflectometer (TSD) is a device used for pavement deflection measurements and is investigated here in numerical simulations as a means of bridge damage detection. A TSD vehicle model containing two displacement sensors is simulated crossing a simply supported finite element beam containing damage simulated as a loss in stiffness of one of the elements. An adapted Cross Entropy optimisation algorithm procedure is proposed to determine the apparent profile, where the displacements recorded by the sensors are used as the inputs. The time-shifted difference in the apparent profile is used as the damage indicator. Results show that this can be reliably used as a damage indicator in the presence of noise and changes in the transverse position of the vehicle on the bridge.

Keywords: bridge, damage, highway, speed, traffic speed deflectometer, TSD, RWD, optimisation, time-shifted.

1. Introduction

Owing to the shortcomings in visual inspections, in recent years there has been a move towards sensor based monitoring of bridge condition. More recently, a small number of authors have shifted to the instrumentation of a passing vehicle, rather than the bridge, in order to assess bridge condition. This approach is referred to as 'drive-by' bridge inspection (Kim and Kawatani, 2009). For short-medium span bridges, there is a good probability that only one truck will be present at a time given the minimum gap between trucks is one to two seconds (corresponding to 20-40 m for a typical speed of 20 ms^{-1}). It is reasonable therefore to believe that the instrumented passing vehicle will not be contaminated by other heavy

traffic on the bridge. Therefore bridge monitoring of this nature does not require lane closures, thus reducing traffic delays and traffic management costs and improving levels of safety. Also, the bridge itself does not need to be instrumented, and so the concept has the potential to be far more cost effective than traditional Structural Health Monitoring.

The feasibility of using a moving vehicle fitted with sensors to extract the first natural frequency of a bridge has been verified in numerical studies and field tests (Yang et al., 2004a; Lin and Yang, 2005; Oshima et al., 2008). The use of drive-by methods for bridge health monitoring, rather than bridge frequency detection has been developed by Kim and Kawatani (2009), McGetrick et al. (2010a) and Toshinami et al. (2010). Later, Yabe and Miyamoto (2012) use the mean displacement of the rear axle of a city bus passing over a bridge a large number of times as a damage indicator.

McGetrick et al. (2009) investigate the effect of a road profile on the feasibility of using an instrumented quarter-car in numerical simulations to detect bridge natural frequencies. Results indicate that the approach works well in the absence of a road profile. However, when an ISO Class 'A' (ISO 8608: 1995) road profile is included in simulations, the bridge frequencies are only detected for speeds of up to 5 m s^{-1}. The road surface roughness excites the vehicle to greater amplitudes than that of the bridge and poses challenges in identifying bridge frequencies (González et al., 2012). While the move to using drive-by methods for damage detection has potential, a significant shortcoming is the need for the vehicle to travel at moderate speeds (González et al., 2008a; Cerda et al., 2012; McGetrick et al., 2013; Lin and Yang, 2005; Toshinami et al., 2010).

Many bridge damage detection methods use Fourier analysis as the principal signal-processing tool (Staszewski and Robertson, 2007). However, Fourier analysis has several shortcomings; it is unable to accurately represent non-periodic functions (Pines and Salvino 2006), non-stationary functions (Qian and Chen, 1999) and it requires linearity. This is a challenge as available data in the 'drive-by' context is from a nonlinear system (Huang et al., 1998), measured signals where structural damage is present are of a non-stationary nature (Staszewski and Robertson, 2007) and the signals are short in duration (Kim and Melhem, 2004). The Short Time Fourier Transform (STFT) was developed for processing non-stationary signals. It involves applying the Fourier Transform to a section of signal known as a window. The width of the window remains constant throughout the analysis and therefore represents a compromise between time and frequency-based views of a signal. Cerda et al. (2012) use a scale model of a vehicle traversing a simply supported beam to experimentally validate the drive-by concept and vertical acceleration signals are processed using the STFT. Results show that low vehicle speeds are needed to accurately identify changes in bridge natural frequency.

The Wavelet Transform, a windowing technique with variable frequencies, represents the next logical step in the development of signal processing methods. A variety of *basis* functions, such as the Haar, the Mexican hat, the Coiflet, the Daubechies and the Morlet, can be used (Kim and Melhem, 2004). However, the transform still suffers from the convolution of the signal with an *a priori* basis function (Ayenu-Prah and Attoh-Okine, 2009), as

available wavelet dictionaries are often not appropriate for analysing the nonlinear behaviour of many structural systems (Salvino et al., 2005).

Engaging in drive-by damage detection at highway speeds has other potential advantages. The higher the speed of the vehicle, the more excited the bridge will become, which could result in the bridge frequency being detected more easily. The challenge is that the data recorded by the vehicle (during the short time it will be on the bridge) will be shorter at higher speeds, capturing only a short segment of the whole period of oscillation. The limitations on VBI in detecting the modal properties of a bridge cannot be overcome by increasing the scanning frequency of the sensors (Keenahan et al., 2014). The underlying problem is that the bridge undergoes very few periods of vibration at its fundamental frequency in the time it takes a vehicle to cross it. Therefore, the only practical solution, if standard signal processing is to be used, is to decrease the velocity of the vehicle to capture more oscillations.

As an alternative to standard signal processing techniques, system identification approaches have become more common in recent years due to advances in signal analysis and information processing techniques. Belay et al. (2008) use the Cross Entropy (CE) method of optimisation to back-calculate vehicle parameters in a study to predict a history of dynamic load. Dowling et al. (2012) use an adapted CE optimisation method to develop a calibration procedure for a Moving Force Identification algorithm. The general system global mass and stiffness matrices of the bridge FE model are found by best fit optimisation to match field measurements. Harris et al. (2010) present a novel method for the characterisation of pavement roughness through an analysis of vehicle accelerations. A combinatorial optimisation technique is applied to the determination of pavement profile heights based on measured accelerations at and above the vehicle axle.

Other authors have used these soft computing techniques for structural damage detection. He et al. (2012) propose a damage detection approach using traffic induced vibration data of a bridge and apply the Genetic Algorithm to identify the damage pattern. A theoretical indirect identification method is proposed by Li et al. (2014) based on an optimisation method rather than the conventional transforms from time domain to frequency domain. Implementation is performed by the Generalised Pattern Search Algorithm and can identify the parameters of the vehicle-bridge system, including the bridge stiffness and the first natural frequency. OBrien and Keenahan (2014) propose an optimisation method as an alternative to standard signal processing techniques. The approach uses a beam in free vibration showing that global damage can be detected.

The recently developed prototype Rolling Weight Deflectometer (RWD), presented first by Briggs et al. (2000) in the United States, is the first move towards the development of a vehicle model designed specifically for ‘drive-by’ inspections of road pavements. The ‘Traffic Speed Deflectometer’ (TSD), is a state of the art device capable of performing deflection surveys at speeds of up to 80 km h^{-1}, avoiding traffic disruption and expensive traffic management. The TSD is a collection of non-contact lasers mounted at equal spacing on a rigid beam, housed in the trailer of an articulated lorry that directly, continuously and

very accurately measures deflections at highway speeds. These deflections have been successfully used as indicators of bearing capacity in pavements damage detection (Briggs et al., 2000). Performing surveys at highway speeds enables high levels of road coverage, greatly reducing costs.

In numerical VBI simulations, this research is the first to investigate using the TSD in a drive-by bridge damage detection context using optimisation to infer the road profile as a damage indicator. The raw output from the TSD is not sensitive to damage as there is significant interference from the vehicle and bridge dynamic interaction. An optimisation approach is proposed as an alternative to standard signal processing techniques to overcome the challenges of the short signal. Five different levels of damage are considered, and the approach allows for noise in the signal and variation in the transverse position of the vehicle in its track.

2. Concept of using the apparent profile as a bridge damage indicator

The TSD vehicle is modelled here as a 4 m long half-car crossing a 100 m approach length followed by a 20 m simply supported FE beam containing an ISO Class 'A' (ISO 8608: 1995) road profile (Figure 1). The 4 degree-of-freedom half-car travels at a constant speed of 20 m s^{-1}. The four independent degrees of freedom correspond to sprung mass bounce displacement, y_s, sprung mass pitch rotation, θ_s and axle hop displacements of the unsprung masses, $y_{u,1}$ and $y_{u,2}$ at axles 1 and 2 respectively. The vehicle body mass is represented by the sprung mass, m_s, and the axle components are represented by unsprung masses, $m_{u,1}$ and $m_{u,2}$. The sprung mass connects to the axle masses via a combination of springs of linear stiffness $k_{s,i}$ and viscous dampers with damping coefficients, $C_{s,i}$ which represent the suspension components for the front and rear axles respectively (i = 1,2). The axle masses then connect to the road surface via springs with linear stiffness, $k_{t,i}$ which represent the tyre components for the front and rear axles (i = 1,2). All the property values of the half-car are listed in Table 1 and are based on values gathered from the literature (Cebon, 1999; Harris et al., 2010). The geometry is obtained from a manufacturer specification for an 18 tonne two-axle truck (DAF Trucks Limited, 2012).

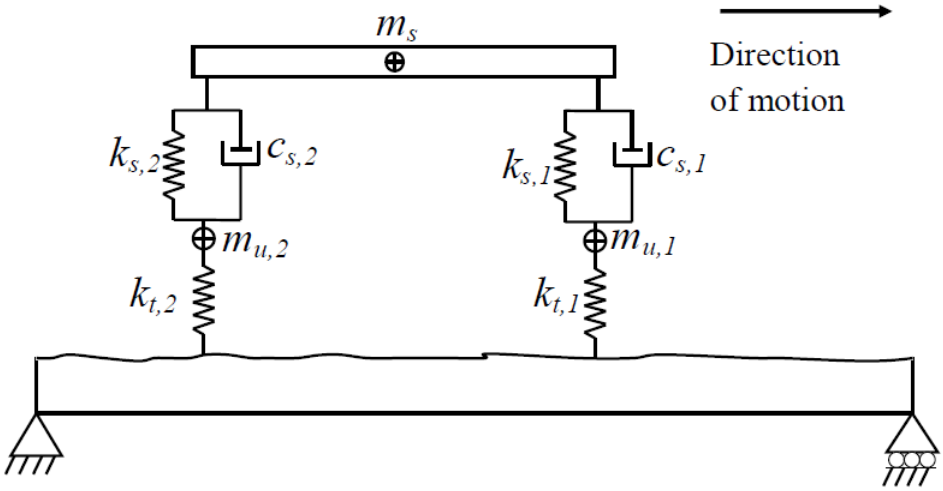

Figure 1: TSD Vehicle Model

Table 1: Half-car properties

Property	**Symbol**	**Value**	**Unit**
Body Mass	m_s	18 000	kg
Axle masses	$m_{u,1}$, $m_{u,2}$	700	kg
Suspension stiffness	$k_{s,1}$, $k_{s,2}$	400 000	N m^{-1}
Suspension Damping	$C_{s,1}$, $C_{s,2}$	10 000	Ns m^{-1}
Tyre Stiffness	$k_{t,1}$, $k_{t,2}$	1.75×10^{6}	N m^{-1}
Moment of Inertia	I_s	9.55×10^{-4}	kg m^2
Distance of axle to centre of gravity	D_1, D_2	2	m

The equations of motion of the vehicle model are obtained by imposing equilibrium of all forces and moments acting on the vehicle and expressing them in terms of the degrees of freedom. They are given by

$$\mathbf{M_v}\ddot{\mathbf{y}}_\mathbf{v} + \mathbf{C_v}\dot{\mathbf{y}}_\mathbf{v} + \mathbf{K_v}\mathbf{y_v} = \mathbf{f_v} \qquad (1)$$

where $\mathbf{M_v}$, $\mathbf{C_v}$ and $\mathbf{K_v}$ are the mass, damping and stiffness matrices of the vehicle respectively. The vectors, $\mathbf{y_v}$, $\dot{\mathbf{y}}_\mathbf{v}$ and $\ddot{\mathbf{y}}_\mathbf{v}$ are the vehicle displacements, their velocities and accelerations respectively. The displacement vector of the vehicle is, $\mathbf{y_v} = \{y_s, \theta_s, y_{u,1}, y_{u,2}\}^\mathbf{T}$. The vector $\mathbf{f_v}$ contains the time varying interaction forces applied by the vehicle to the bridge: $\mathbf{f_v} = \{0 \quad 0 \quad -F_{t,1} \quad -F_{t,2}\}^\mathrm{T}$. The term $\boldsymbol{F_{t,i}}$, represents the dynamic interaction force at wheel i:

$$F_{t,i} = k_{t,i}(y_{u,i} - y_{br} - r_i) \quad (2)$$

where y_{br} is the deflection of the bridge and r_i is the road profile height. Cebon (1999) describes how an artificial road surface topography can be generated stochastically based on the (ISO 8608: 1995) method of representing road surface roughness with a power spectral density function and then applying the inverse Fast Fourier Transform. A class 'A' road profile (Figure 2), a very good profile, as expected in a well maintained highway, is considered and has a geometric spatial mean of 8×10^{-6} m^3 cycle^{-1}. The profile in Figure 2 is 124 m in length as this allows for the second axle to leave the bridge (axle spacing is 4 m). A moving average filter is applied to the generated road profile heights, $\boldsymbol{r_i}$, over a distance of 0.24 m to simulate the attenuation of short wavelength disturbances by the tyre contact patch (Harris et al. 2007).

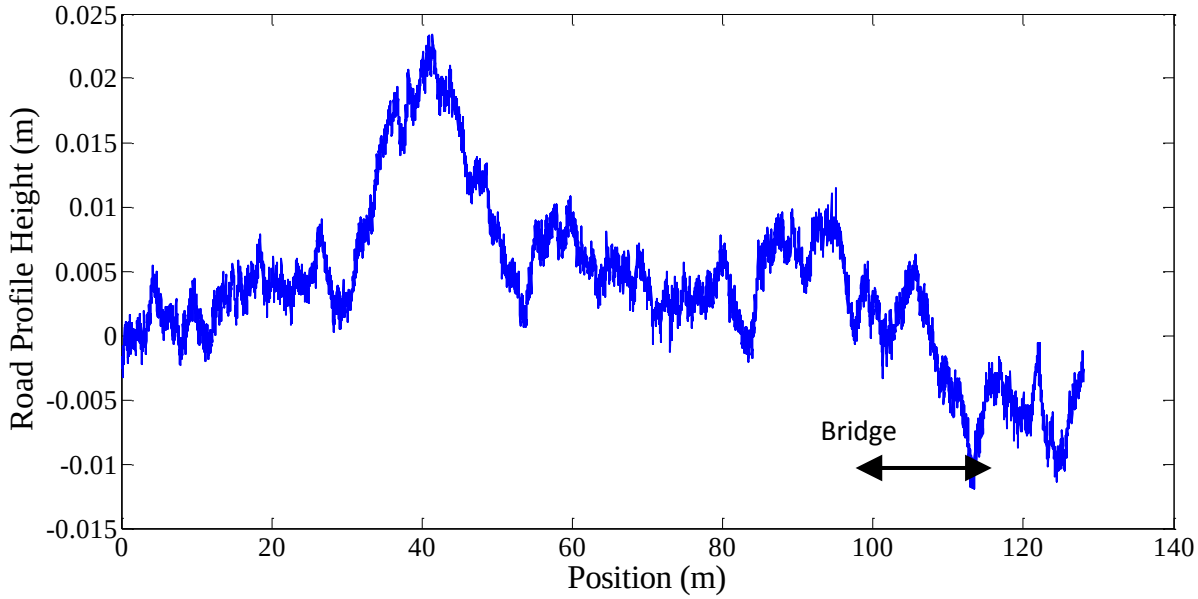

Figure 2: Road profile

The bridge is simulated as a 20 m simply supported FE beam model. It consists of 20 discretised beam elements with 4 degrees of freedom. Therefore the beam model has a total of n = 42 degrees of freedom. The beam has a modulus of elasticity of $E = 35 \times 10^9$ N m^{-2}, the density is ρ = 2446 kg m^{-2}, the second moment of area is taken as J = 0.3333 m^4 and the bridge damping ratio is 3%. The response of the discretised beam model to moving time-varying forces is given by the system of equations:

$$\mathbf{M_b}\ddot{\mathbf{y}}_\mathbf{b} + \mathbf{C_b}\dot{\mathbf{y}}_\mathbf{b} + \mathbf{K_b}\mathbf{y_b} = \mathbf{N_b}\mathbf{f_{int}} \quad (3)$$

where $\mathbf{M_b}$, $\mathbf{C_b}$ and $\mathbf{K_b}$ are the global mass, damping and stiffness matrices of the beam model respectively. The terms $\ddot{\mathbf{y}}_\mathbf{b}$, $\dot{\mathbf{y}}_\mathbf{b}$ and $\mathbf{y_b}$ are the vectors of nodal bridge accelerations, velocities and displacements respectively. The product, $\mathbf{N_b}\mathbf{f_{int}}$, is the vector of forces applied to the bridge nodes. The vector, $\mathbf{f_{int}}$, contains the interaction forces between the vehicle and the bridge and is described by:

$$\mathbf{f_{int}} = \mathbf{P} + \boldsymbol{F_{t,i}} \quad (4)$$

where **P** is the static axle load vector the vector and $\boldsymbol{F_{t,i}}$ contains the dynamic wheel contact forces of each axle. The role of $F_{t,i}$ is to provide a link between the moving forces and the bridge structure. It is determined from Eq. (2) which is a product of the tyre stiffness and the tyre displacement at each moment in time. The tyre displacement is calculated by subtracting the bridge displacement and road profile height from the axle displacement at each moment in time. The location matrix, $\mathbf{N_b}$, distributes the applied interaction forces on beam elements to equivalent forces acting on nodes. This location matrix can be used to calculate bridge displacements under each wheel, $\mathbf{y_{br}}$:

$$\mathbf{y_{br}} = \mathbf{N_b^T}\,\mathbf{y_b} \tag{5}$$

Although complex damping mechanisms may be present in the structure, viscous damping is typically used for bridge structures and is deemed to be sufficient to reproduce the bridge response accurately. Therefore, Rayleigh damping is adopted here to model viscous damping. With Rayleigh damping, the system damping matrix is a function of the bridge mass and stiffness matrices and is deemed to be unaffected by the applied loading:

$$\mathbf{C_b} = \alpha\mathbf{M_b} + \beta\mathbf{K_b} \tag{6}$$

where α and β are constants. The damping ratio is assumed to be the same for the first two modes (Yang et al., 2004b) and α and β are obtained from $\alpha = 2\,\xi\,\omega_1\omega_2/(\omega_1 + \omega_2)$ and $\beta = 2\,\xi\,/(\omega_1 + \omega_2)$ where ω_1 and ω_2 are the first two natural frequencies of the bridge (Clough and Penzien, 1975).

The dynamic interaction between the vehicle and the bridge is implemented in MatLab. The vehicle and the bridge are coupled at the tyre contact points via the interaction force vector, $\mathbf{f_{int}}$. The equations for the coupled system are solved using the Wilson-Theta integration scheme (Bathe and Wilson, 1976; Tedesco et al., 1999). The optimal value of the parameter θ = 1.420815 is used for unconditional stability in the integration schemes (Weaver and Johnston, 1987). The scanning frequency used for all simulations is 1000 Hz.

Damage is modelled as recommended by Sinha et al. (2002) where a crack causes a loss in stiffness over a region of 3 times the beam depth, varying linearly from a maximum at the centre. Damage is included here in the 14th element, i.e., about one third of the length from the right hand support. The healthy case has a reduction in beam depth of 0, and the most damaged case (50% damage) has a beam depth reduction of 0.5 m. The sensitivity of the apparent profile to damage is investigated first. The vehicle is simulated crossing the bridge with the known profile of Figure 2 at two levels of damage (0% and 20%). The bridge displacement for each of these damage levels is added to the true road profile and adds a few millimetres to give the apparent profile, i.e., the profile that would be measured from a datum fixed in space (Figure 3).

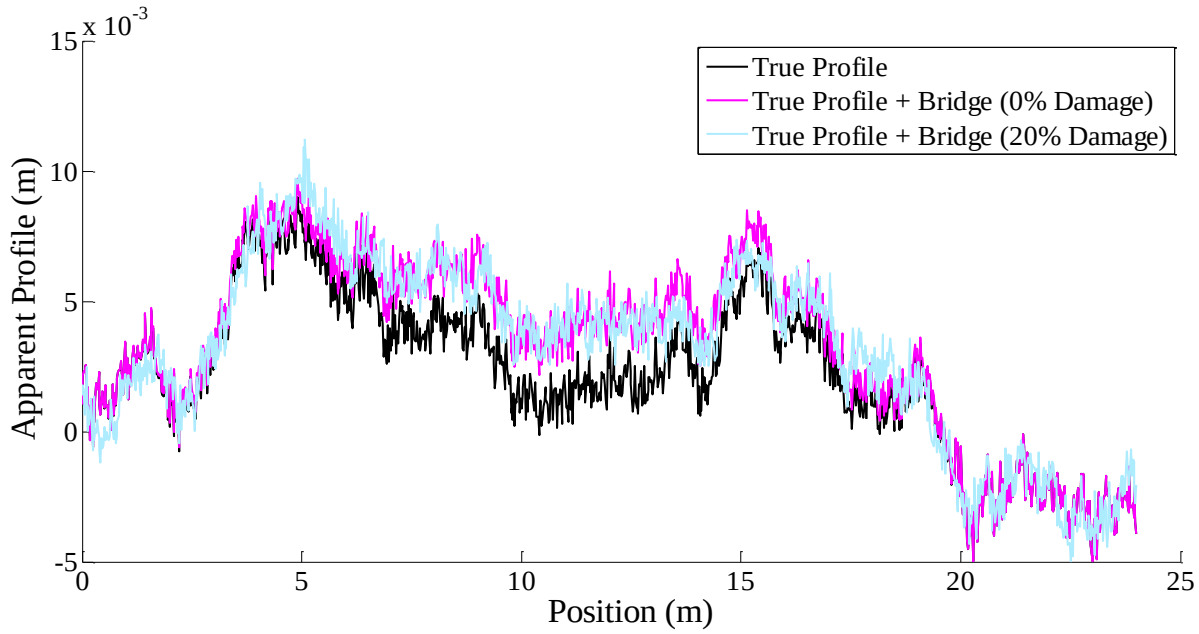

Figure 3: Influence of bridge deflections on the inferred profile

The black curve is the plot of the true profile. There is a clear distinction between this curve, and the apparent profile (pink/ grey one), where deflections from a healthy bridge have been included. There is a further distinction with the second apparent profile (light blue/ grey one), where deflections from a damaged bridge have been added to the true profile during the vehicle crossing event. Therefore, provided that the apparent profile can be determined with a greater accuracy than the difference in the above curves, bridge damage may be detected from changes in the apparent profile.

3. Adapted CE optimisation method

The apparent profile will be calculated here using Cross Entropy (de Boer et al., 2005) optimisation to find the profile elevations that give the best fit of theoretical to measured TSD deflection measurements. The TSD measures the distance from a straight line on the vehicle to the road surface over the bridge. These distances are directly related to the road profile and bridge elevation at the time of measurement. They are also affected by vehicle bouncing and rocking motions and, as the vehicle is excited by the profile, these components are indirectly related to the apparent profile. Using a calibrated vehicle, unknown road profiles are found by optimising to find the elevations which replicate the measured response.

The first step in the CE algorithm is to generate an initial population of values for each of the unknown road profile elevations. If there are n points at which profile elevations are required, then p trial solutions are stored in the $n \times p$ matrix [r]. Each elevation is taken to be Normally distributed and is therefore defined by its mean and standard deviation. Hence the population of p profiles can be characterised by vectors of mean and standard deviation, μ_r and σ_r. A population of p trial road profiles are randomly generated using initial values for μ_r and σ_r. For each profile in the population, a VBI simulation calculates displacements as measured by

the vehicle. The objective function, O_i is defined as the sum of the squares of the differences between displacements, y_i calculated for each trial profile, i, and the measured displacements, y_i^{ME}:

$$O_i = \sum(y_i(\boldsymbol{r_i}) - y_i^{ME})^2 \quad (7)$$

where $\boldsymbol{r_i}$ is the i^{th} row of the matrix, [r]. The vector of p objective functions is ranked and the 10% of trial profiles that give the lowest objective function value are identified. This 'elite set' (Rubinstein and Kroese, 2004) is retained to regenerate the population. With the means and standard deviations of this elite set, μ_r' and σ_r', Monte Carlo simulation is used to generate the population for the next generation of trial profiles. A tolerance is specified to establish when convergence has been reached, in this case, 0.005% difference in successive population means. A common problem with the CE algorithm is that it may converge prematurely to a false solution. Botev et al. (2005) propose the method of 'injecting' extra variance into the samples and restarting to address this problem. This technique, also used here, 'widens' distributions and reduces premature convergence.

Given the large number of unknowns in the problem, an adapted version of the CE method is used. The optimisation is split into a number of phases, in which a smaller 'window' of the road profile is determined before proceeding to the next phase (Figure 4). This means that only n unknowns need to be considered at any one time, significantly reducing the dimensionality of the problem.

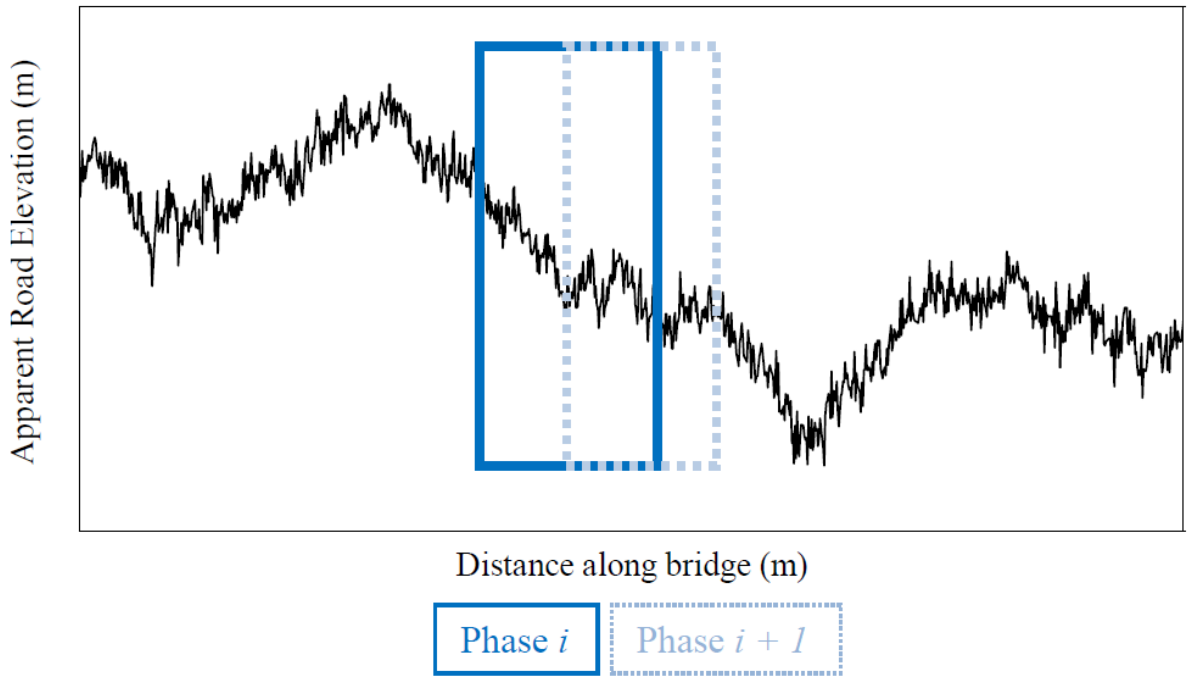

Figure 4: Windows of apparent road surface profile

At the end of each phase, the first $\frac{n}{2}$ profile heights are saved as the apparent profile, and the remaining half of the profile heights are used as the first $\frac{n}{2}$ 'means' for the next phase of n unknowns (Figure 4). The remaining $\frac{n}{2}$ mean values for the next phase are taken as the n^{th} mean from the previous phase. The standard deviation is always reset here as an array going from 0.1 in increments of $\frac{1}{n}$ to 1. The process continues until the profile heights in each phase have been determined. This is to reflect the relative uncertainty in estimates further along the window being analysed.

A further adaption of the CE optimisation process used here is in the sub-structuring of the problem. Each unknown is substantially independent of the other unknowns and therefore objective sub-functions can be defined (Dowling et al. 2012). The objective sub-functions are defined as the squared differences between each of the n displacements calculated for each of the p trial profiles, $\mathrm{d}_{\mathrm{i_C}}$, and each of the n displacements from the measured profile, $\mathrm{d}_{\mathrm{i_M}}$

$$\left(\mathrm{d}_{\mathrm{i_C}} - \mathrm{d}_{\mathrm{i_M}}\right)^2 \forall\, i = 1,2,\ldots n \tag{8}$$

This is different from conventional CE in that the overall objective function can be split into objective sub-functions. For each iteration the objective sub-functions are ranked and the 10% of trial profiles that give the lowest objective sub-function value are identified. This 'elite set' (Rubinstein and Kroese, 2004) is retained to regenerate the population. With the means and standard deviations of each component of this elite set, Monte Carlo simulation is used to generate the population for the next generation of trial profiles. The process for finding a set of unknown profile heights is presented in Figure 5.

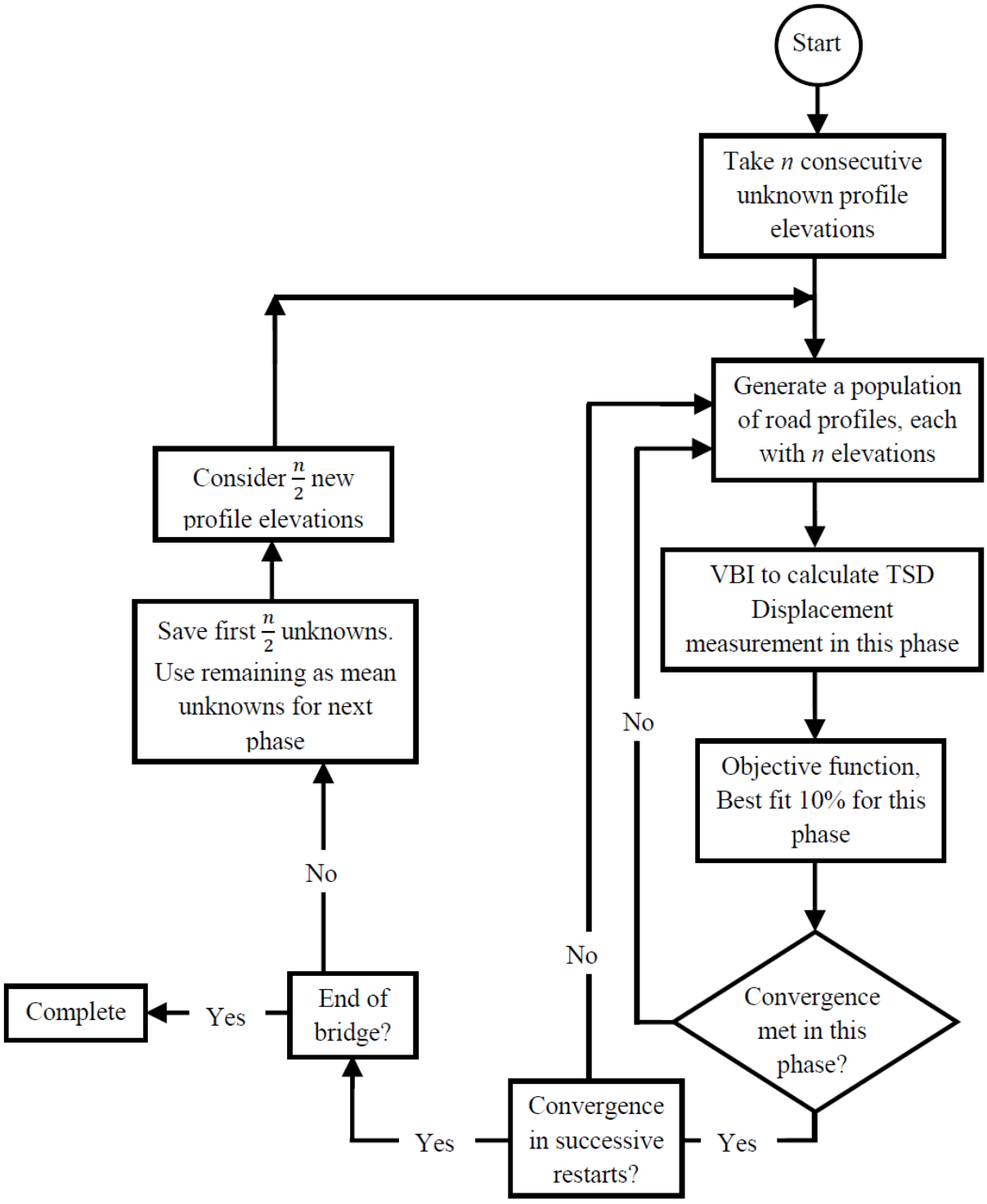

Figure 5: Flow chart of algorithm to find apparent profile

4. Using optimisation to infer the profile

The TSD vehicle model from Section 3 is now modelled crossing a 20 m ISO Class 'A' (ISO 8608: 1995) road profile with no bridge present. Two sensors are simulated; one at the front of the vehicle and one at the rear (Figure 6). It is assumed that the two sensors measure the

distance of the vehicle to from the surface which includes elements of the road profile heights and the bounce and pitch motions of the vehicle. The displacements read by each sensor, h_A and h_B, are given by Eq. (9) and (10), where the vehicle height above the ground, h, is taken to be 0.5 m;

$$h_A = h - bounce - b * pitch - road_A \quad (9)$$

$$h_b = h - bounce + b * pitch - road_b \quad (10)$$

at a given instant in time, where $road_A$ and $road_B$ are the road profile heights read by sensors A and B respectively.

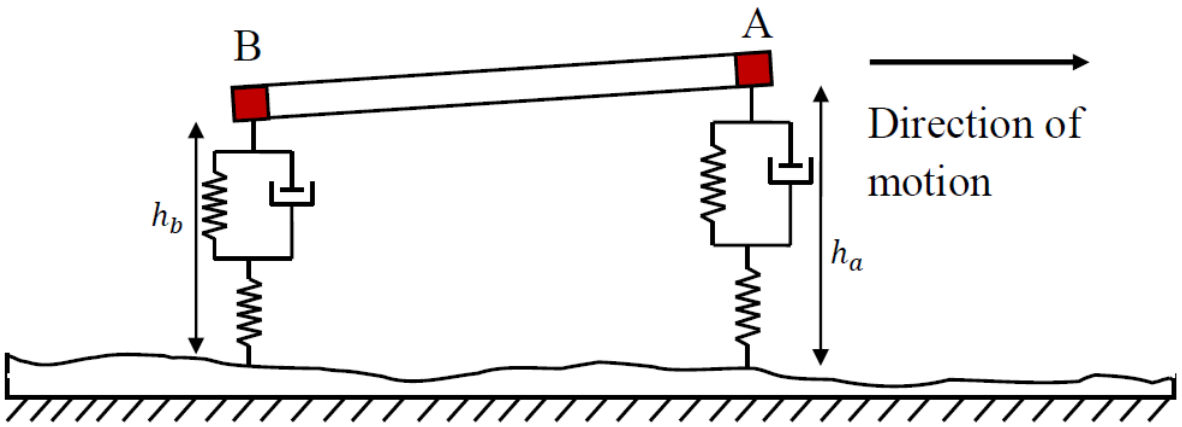

Figure 6: Half-car on a road profile

The vehicle model traverses the known road profile to determine the 'measured' response, i.e., the displacements that would be read by each of the sensors on the vehicle. Using a calibrated vehicle, the unknown road profile heights are determined by optimising to find the road profile which best replicates the measured response. This is done using the combinatorial optimisation method described in Section 3. The number of unknown profile elevations '*n*' considered in each window is 10 and the population size (number of alternative profile segments), *p*, is 150. A value of n = 10 was chosen as a compromise between computational inefficiency (low value of *n*) and risk of optimisation errors (large value of *n*). The true profile and inferred profile are almost identical as can be seen by the error in the inferred profile, presented in Figure 7.

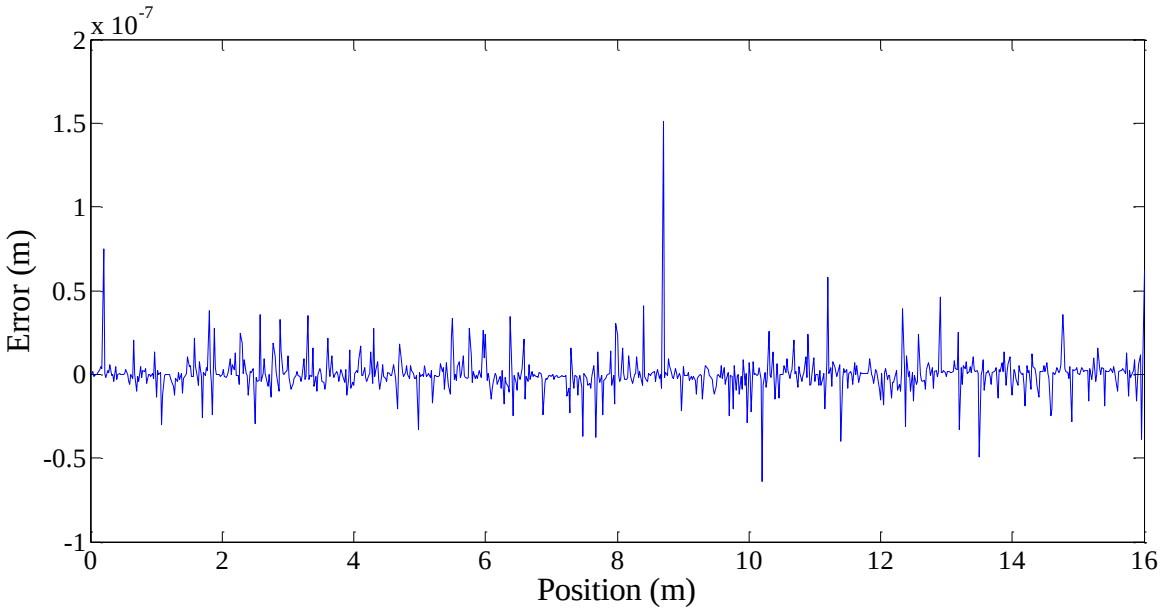

Figure 7: Error in the inferred profile

The error in the inferred profile is of the order of $\times 10^{-7}$. The expected error in the inferred profile, due to bridge damage, as illustrated in Figure 3, is of the order of $\times 10^{-3}$. Provided that the inferred profile can be determined with a similar level of accuracy as above, in the presence of a full VBI, then it should be possible to detect damage.

5. Bridge damage detection using the inferred profile found using CE optimisation

The TSD vehicle model is simulated crossing a 100 m approach length followed by a 20 m bridge, containing a profile. As described in Section 2, damage is included in the 14th out of 20 elements through a local loss of stiffness (Sinha et al. 2002). The optimisation procedure outlined in Section 3 is used again here to find the inferred profile, using the data read by the sensors as the measured response. The sensors are now reading the height from the vehicle to the ground, the profile heights, vehicle pitch and bounce motions, as well as the bridge displacements. The apparent profile found by optimisation only includes profile heights and bridge displacements. The apparent profile found by the first sensor for the six damage levels can be seen in Figure 8. Figure 9 illustrates a portion of Figure 8 that has been re-scaled for clarity.

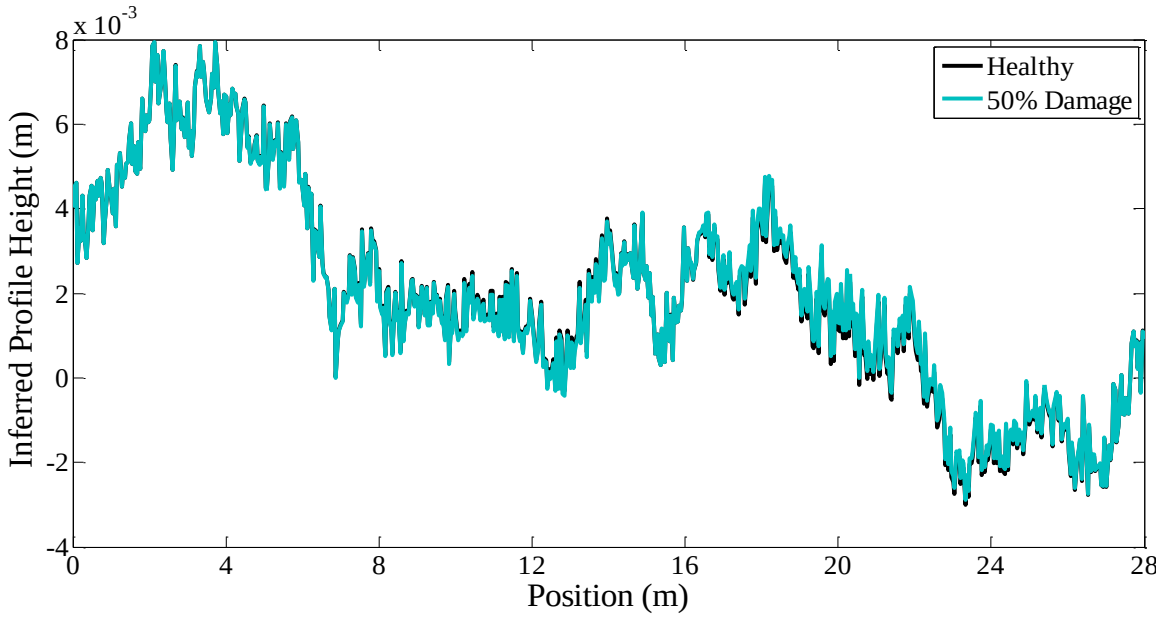

Figure 8: Apparent profile for sensor one with two levels of damage

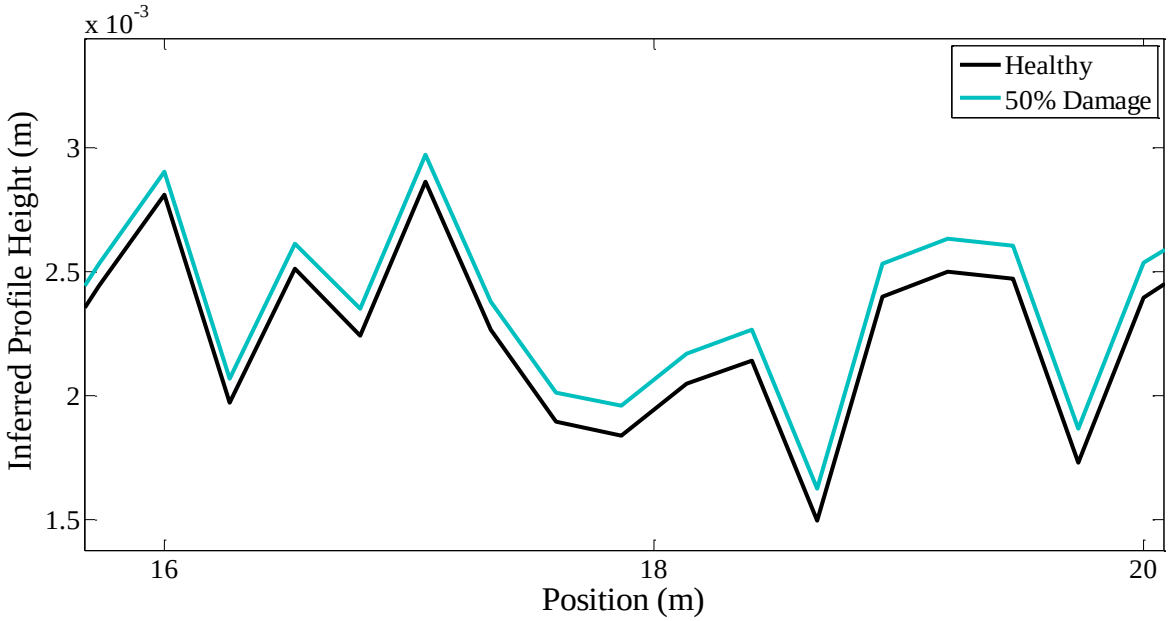

Figure 9: Re-scaled apparent profile

It is clear from this figure that damage cannot be easily detected from the inferred profile.

The measurements for each of the two sensors can be used independently to find apparent profiles. The road profile components are identical in each case but the contributions of bridge displacements are different as the sensors cross the bridge at different times. Therefore, subtracting the apparent profiles gives an 'error' function that is inferred only by bridge vibration. This time-shifted difference in bridge displacements is represented as:

$$\kappa = y_i - y_{i-\Delta} \tag{11}$$

where Δ is the number of elevations corresponding to the distance between the axles. The time-shifted difference in bridge displacements is plotted in Figure 10 for a range of damage levels.

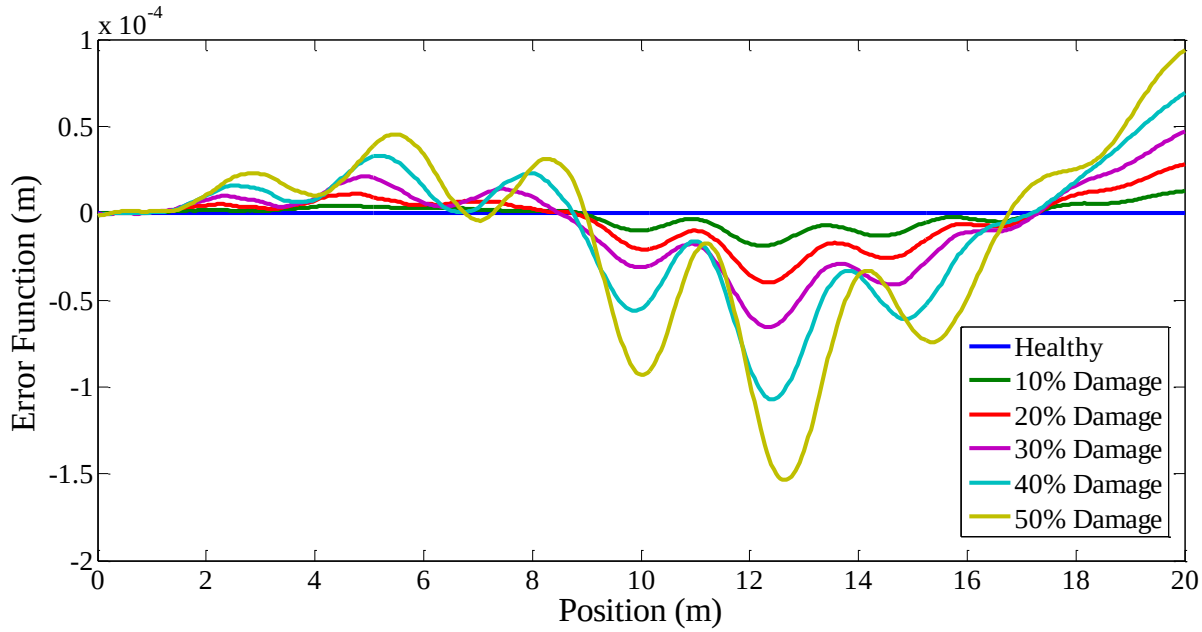

Figure 10: Time-shifted difference in inferred profiles

It is clear from Figure 10 that provided it can be accurately calculated, damage can be identified using the time-shifted difference in apparent profiles (the error function). The time shifted difference is sensitive to damage because, with the influence of road profile removed, the bridge vibration is the dominant influencing factor. While the magnitude of the error function is small, the accuracy of Traffic Speed Deflectometers is excellent and manufacturers claim a repeatability of measurements of 20 microns. The approach also investigated damage in different locations to see if there was a correlation between the peaks in the time-shifted difference in apparent profiles and location of damage, however this work was inconclusive.

6. Influence of noise and changes in the transverse position of the vehicle on the bridge

Thus far, the TSD has been simulated crossing the same single track of a randomly generated road profile. A carpet profile (Figure 11) is generated from the initial road profile, correlating adjacent profiles transversely (Cebon & Newland 1983). The carpet profile generated has eleven alternative paths, and for each simulation, the path through the carpet is selected according to an assumed truncated normal distribution for transverse location.

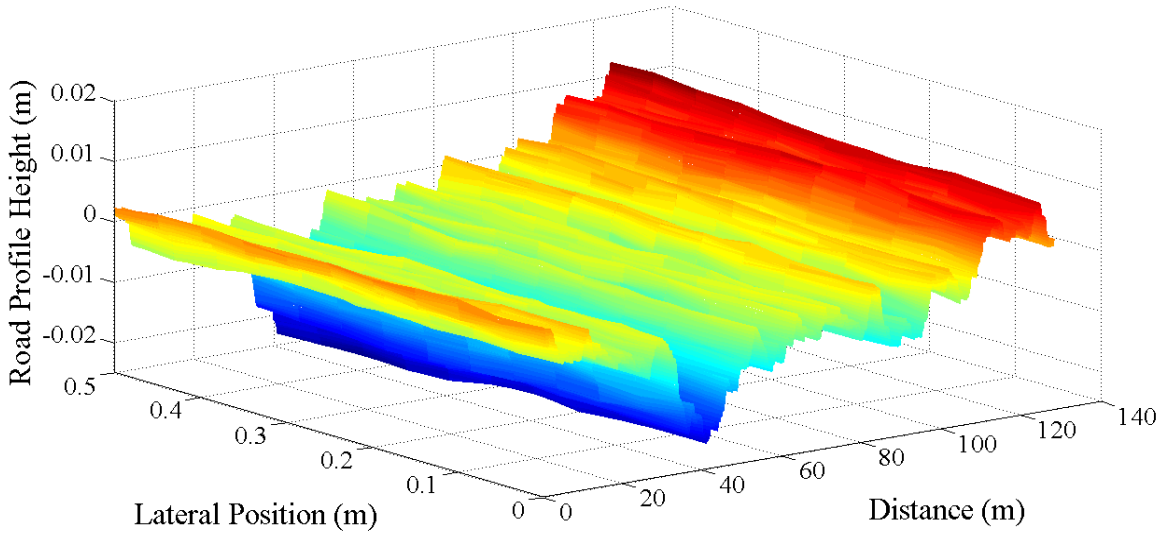

Figure 11: Carpet profile

Additive White Gaussian Noise (AWGN), according to Lyons (2011), is added to the 'measured' displacements read by each sensor before being used in the optimisation procedure:

$$D_{poll} = D + E_{noise} * N \tag{12}$$

where D_{poll} is the signal containing noise, D is the original signal containing no noise, N is a standard normal distribution vector with zero mean and unit standard deviation and E_{noise} is the energy in the noise. The term, E_{noise}, is determined from the definition of the Signal to Noise Ratio (*SNR*) given by:

$$SNR = 10\, log_{10} \frac{var\,(D)}{E_{noise}^2} \tag{13}$$

which is the ratio of the power in the signal to the power in the noise and *var(D)* is the variance of the signal. In these simulations, the *SNR* is specified, and *var (D)* is easily determined. Using Eq. (13), noise at an SNR level of 65 is added to the beam displacements. This corresponds to noise of 5 microns reflecting the level of accuracy that might be expected from a TSD. As before, the TSD traverses the bridge six times, once for the healthy case and once for each of the five damage levels. Each time the TSD crosses the bridge, it traverses a randomly selected path through the carpet profile and a different noise is added. The displacements are read by each of the two sensors, and the optimisation procedure is then used to determine the inferred profiles. The time-shifted difference in inferred profiles can be seen in Figure 12.

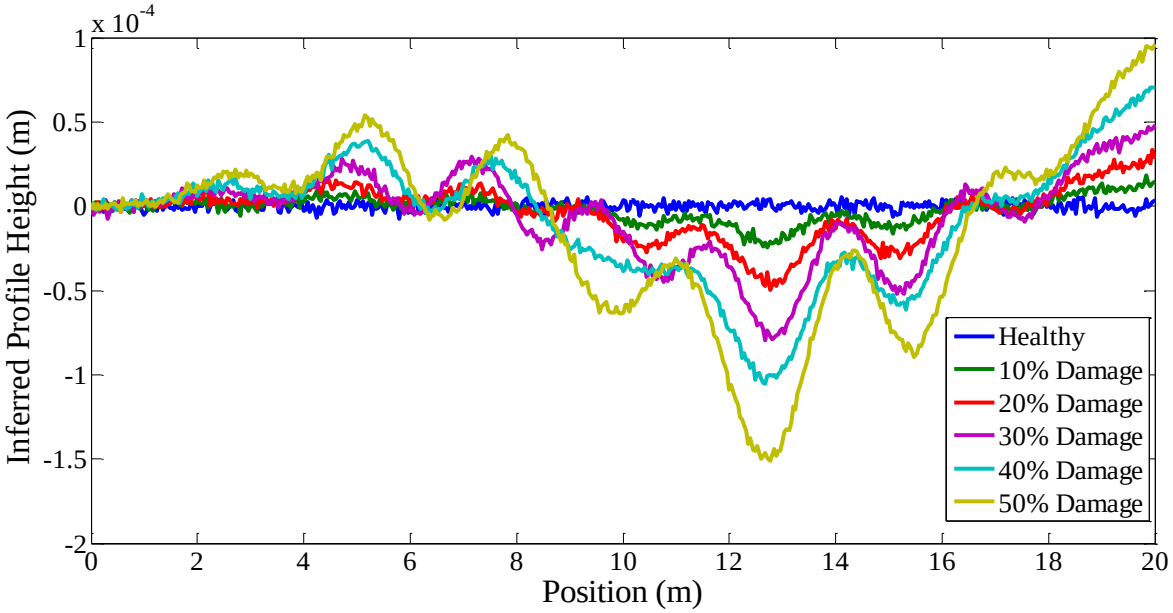

Figure 12: Time-shifted difference in inferred profiles in the presence of noise and changes in transverse position of the vehicle on the bridge

7. Discussion and Conclusion

This work investigates the feasibility of using a Traffic Speed Deflectometer for drive-by damage detection for short-medium span bridges. The concept of drive-by damage detection is to determine a health rating rapidly, at low cost and with minimum disruption to traffic. It is reasonable to believe that the Traffic Speed Deflectometer will not be influenced by other heavy traffic on the bridge. As such, we do not propose any lane closures and would suggest that the measurement be repeated if it is 'contaminated' by the presence of another heavy vehicle. The data gathered from the TSD is used as the measured response in an adapted Cross Entropy optimisation procedure. The optimisation infers the road profile, twice, using two different sensors, and the time-shifted difference in apparent profiles is used as the damage indicator. Damage can be clearly seen, even for low levels of damage. For the first time, damage detection in bridges can be effectively carried out at highway speeds in the Drive-by context, without contamination from the road profile, using just two sensors.

Acknowledgements

The authors wish to express their gratitude for the financial support received from Science Foundation Ireland towards this investigation under the US-Ireland Research Partnership Scheme.

8. References

Ayenu-Prah, A. & Attoh-Okine, N., 2009. Comparison study of hilbert-huang transform, fourier transform and wavelet transform in pavement profile analysis. *Vehicle System Dynamics*, 47(4), pp.437–456.

Bathe, K.J. & Wilson, E.L., 1976. *Numerical methods in finite element analysis*, Englewood Cliffs, New Jersey, NJ, USA: Prentice-Hall.

Belay, A., OBrien, E.J. & Kroese, D., 2008. Truck fleet model for design and assessment of flexible pavements. *Journal of Sound and Vibration*, 311(3-5), pp.1161–1174.

De Boer, P.-T., Kroese, D., Mannor, S. & Rubinstein, R., 2005. A Tutorial on the Cross-Entropy Method. *Annals of Operations Research*, 134(1), pp.19–67.

Botev, Z., Kroese, D.P., Maonr, S. & Rubinstein, R.Y., 2005. Global likelihood optimization via the Cross-Entropy method, with an application to mixture models. In R. G. Ingalls, M. D. Rossetti, J. S. Smith, & H. A. Peters, eds. *Proceedings of the 2004 Winter Simulation Conference, WSC*. Washington, DC, USA, pp. 529–535.

Briggs, R.C., Johnson, R.F., Stubstad, R.N. & Pierce, L., 2000. A comparison of the rolling weight deflectometer with the falling weight deflectometer. In *Symposium on Nondestructive Testing of Pavements and Backcalculation of Moduli: Third Volume*. West Conshohocken, PA, USA, pp. 444–456.

Cebon, D., 1999. *Handbook of Vehicle-Road Interaction*, The Netherlands: Swets & Zeitlinger Lisse.

Cebon, D. & Newland, D.E., 1983. Artificial generation of road surface topography by the inverse F.F.T. method. *Vehicle System Dynamics*, 12(1-3), pp.160–165.

Cerda, F., Garrett, J., Bielak, Barrera, J., Zhuang, Z., et al., 2012. Indirect structural health monitoring in bridges: scale experiments. In *Bridge Maintenance, Safety, Management, Resiliance and Sustainability (IABMAS2012)*. Stresa, Italy: CRC Press, Taylor and Francis Group, London, UK, pp. 346–353.

Clough, R.W. & Penzien, J., 1975. *Dynamics of structures*, New York, NY, USA: McGraw-Hill.

DAF Trucks Limited, 2012. FAT CF75 30t Specification sheet. Available at: http://www.atn.co.za/LinkWrap.asp?model_id=14091&filename=/specs/FAT CF75 6X4 RIGID%281%29.pdf&asset_name=D+A+F+FAT+CF75+Truck+Rigid.

Dowling, J., OBrien, E.J. & González, A., 2012. Adaption of cross-entropy optimisation to a dynamic bridge WIM calibration problem. *Engineering Structures*, 44, pp.13–22.

González, A., 2010. Vehicle-bridge dynamic interaction using finite element modelling. In D. Moratal, ed. *Finite Element Analysis*. Sciyo, pp. 637–662.

González, A., Covián, E. & Madera, J., 2008. Determination of bridge natural frequencies using a moving vehicle instrumented with accelerometers and a geographical positioning system. In *Proceedings of the Ninth International Conference on Computational Structures Technology*. Athens, Greece.

González, A., OBrien, E.J. & McGetrick, P.J., 2012. Identification of damping in a bridge using a moving instrumented vehicle. *Journal of Sound and Vibration*, 331(18), pp.4115–4131.

Harris, N.K., Gonzalez, A., Obrien, E.J. & McGetrick, P., 2010. Characterisation of pavement profile heights using accelerometer readings and a combinatorial optimisation technique. *Journal of Sound and Vibration*, 329(5), pp.497–508.

Harris, N.K., OBrien, E.J. & González, A., 2007. Reduction of bridge dynamic amplification through adjustment of vehicle suspension damping. *Journal of Sound and Vibration*, 302(3), pp.471–485.

He, X., Catbas, F.N., Hattori, H., Furuta, H., Kawatani, M., et al., 2012. Development of a bridge damage detection approach using vehicle-bridge interaction analysis and soft computing mothods. In *Bridge Maintenance, Safety, Management, Resiliance and Sustainability*. Stresa, Italy, pp. 392–398.

Huang, N.E., Shen, S., Long, S., Wu, M., Shih, H., et al., 1998. The empirical mode decomposition and the hilbert spectrum for nonliner and nonstationary time series analysis. *Proceedings of the Royal Society of London A*, 454, pp.903–995.

ISO 8608:, 1995. *Mechanical vibration-road surface profiles - reporting of measured data*,

Keenahan, J., OBrien, E.J., McGetrick, P.J. & González, A., 2014. The use of a dynamic truck-trailer drive-by system to monitor bridge damping. *Structural Health Monitoring*, 13(2), pp.183–197.

Kim, C.W. & Kawatani, M., 2009. Challenge for a drive-by bridge inspection. In *Proceedings of the 10th International Conference on Structural Safety and Reliability, ICOSSAR2009*. Osaka, Japan: CRC Press, Taylor and Francis Group, London, UK, pp. 758–765.

Kim, H. & Melhem, H., 2004. Damage detection of structures by wavelet analysis. *Engineering Structures*, 26(3), pp.347–362.

Li, W., Jiang, Z., Wang, T. & Zhu, H., 2014. Optimization method based on Generalized Pattern Search Algorithm to identify bridge parameters indirectly by a passing vehicle. *Journal of Sound and Vibration*, 333, pp.364–380.

Lin, C.W. & Yang, Y.B., 2005. Use of a passing vehicle to scan the fundamental bridge frequencies: an experimental verification. *Engineering Structures*, 27(13), pp.1865–1878.

Lyons, R.G., 2011. *Understanding Digital Signal Processing* Third Edit., Boston, MA, USA: Prentice-Hall.

McGetrick, P.J., González, A. & O'Brien, E., 2010. Monitoring bridge dynamic behaviour using an instrumented two axle vehicle. In *Bridge and Concrete Research in Ireland*. Cork, Ireland.

McGetrick, P.J., González, A. & OBrien, E.J., 2009. Theoretical investigation of the use of a moving vehicle to identify bridge dynamic parameters. *Insight: Non-Destructive Testing & Condition Monitoring*, 51, pp.433–438.

McGetrick, P.J., Kim, C.W., González, A. & OBrien, E.J., 2013. Dynamic axle force and road profile identification using a moving vehicle. *International Journal of Architecture, Engineering and Construction*, 2(1), pp.1–16.

McGetrick, P.J., Kim, C.W. & O'Brien, E.J., 2010. Experimental investigation of the detection of bridge dynamic parameters using a moving vehicle. In *Proceedings of the 23rd KKCNN Symposium on Civil Engineering*. Taipei.

OBrien, E.J. & Keenahan, J., 2014. The analysis of short signal segments and its application to drive-by bridge inspections.

Oshima, Y., Yamaguchi, T., Kobayashi, Y. & Sugiura, K., 2008. Eigenfrequency estimation for bridges using the response of a passing vehicle with excitation system. In *Proceedings of the Fourth International Conference on Bridge Maintenance, Safety and Management, IABMAS2008*. Seoul, Korea: CRC Press, Taylor and Francis Group, London, UK, pp. 3030–3037.

Pines, D. & Salvino, L., 2006. Structural health monitoring using empirical mode decomposition and the Hilbert phase. *Journal of Sound and Vibration*, 294(1–2), pp.97–124.

Qian, S. & Chen, D., 1999. Joint time-frequency analysis. *Signal Processing Magazine, IEEE*, 16(2), pp.52–67.

Rubinstein, R.Y. & Kroese, D.P., 2004. *The cross entropy method*, New York, NY, USA: Springer New York LLC.

Salvino, L.W., Pines, D.J., Todd, M. & Nichols, J.M., 2005. EMD and instantaneous phase detection of structural damage. In N. E. Huang & S. S. Shen, eds. *Hilbert-Huang transform and its applications*. Singapore: World Scientific Publishing., pp. 227–261.

Sinha, J.K., Friswell, M.I. & Edwards, S., 2002. Simplified models for the location of cracks in beam structures using measured vibration data. *Journal of Sound and Vibration*, 251(1), pp.13–38.

Staszewski, W.J. & Robertson, A.N., 2007. Time-frequency and time-scale analyses for structural health monitoring. *Philosophical Transactions of the Royal Society A: Mathematical, Physical and Engineering Sciences*, 365(1851), pp.449–477.

Tedesco, J.W., McDougal, W.G. & Ross, C.A., 1999. *Structural dynamics: theory and applications*, California, CA, USA: Addison Wesley Longman.

Toshinami, T., Kawatani, M. & Kim, C.W., 2010. Feasibility investigation for identifying bridge's fundamental frequencies from vehicle vibrations. In *Proceedings of the Fifth International Conference on Bridge Maintenance, Safety and Management, IABMAS2010*. Philadelphia, USA: CRC Press, Taylor and Francis Group, London, UK, pp. 317–322.

Weaver, W. & Johnston, P.R., 1987. *Structural dynamics by finite elements*, Indiana, USA: Prentice-Hall.

Yabe, A. & Miyamoto, A., 2012. Bridge condition assessment for short and medium span bridges by vibration responses of city bus. In *Bridge Maintenance, Safety, Management, Resiliance and Sustainability (IABMAS2012)*. Stresa, Italy: CRC Press, Taylor and Francis Group, London, UK, pp. 195–202.

Yang, Y.B., Lin, C.W. & Yau, J.D., 2004. Extracting bridge frequencies from the dynamic response of a passing vehicle. *Journal of Sound and Vibration*, 272(3-5), pp.471–493.

Yang, Y.B., Yau, J.D. & Wu, Y.S., 2004. *Vehicle-Bridge Interaction Dynamics: with Applications to High-Speed Railways*, Singapore: World Scientific Publishing Co. Pte. Ltd.